Improved oscillating buoy viscometer

Rogers C. Ritter and Janelle A. Molloy

Physics Department, University of Virginia, Charlottesville, Virginia 22901

(Received 22 May 1987; accepted for publication 1 August 1987)

An improved design of the vertically oscillating buoy viscometer with real-time computer control, evaluation, and plotting is presented. In this method, the optically observed phase lag of the buoy relative to a sinusoidal driving force is a direct and absolute measure of viscosity. Construction features of the new version improve reassembly precision and give three-axis positioning of the sphere, as well as an 80-fold improvement in the signal-to-noise ratio for small amplitudes of the buoy motion. Design of the "crossed coil" system is discussed and the magnetic and mechanical faults which lead to various kinds of motional instability are considered. Boundary layer corrections are now computer corrected as are temperature variations. The evaluation of "intrinsic viscosity" as a measure of molecular ellipticity is discussed and one measurement set is presented.

INTRODUCTION

A magnetically suspended buoy with vertically driven oscillations has a phase and amplitude response which depends strongly on the viscosity of the fluid in which it is immersed. An instrument has been designed and built on this principle,[1] and the amplitude aspect was removed in the method of extracting the data. Subsequently several viscometers based on a similar principle, but with somewhat different goals, have been reported.[2,3]

In our particular development the instrument was used with dilute aqueous biomolecular samples which were transparent, hence optical sensing of the buoy position was appropriate. Essential features included the need for small samples ~ 100 μl, very small stresses on the fluid ($< 10^{-5}$ dyn/cm^2), a precision $\sim 10^{-3}$ and ultimately $\sim 10^{-4}$. It was important that density measurements be made simultaneously on the same sample and that the response time be seconds, or at the most 1 or 2 min. In addition, it was desirable that in some cases the operation be with ultralow buoy motional amplitude, in hopes that we could study mechanical behavior of biological molecules in a new way. When the buoy motion is smaller than the molecular dimensions, one might expect the "viscosity measurement" to take on new meaning.

In the original design most of these goals were met, but there were certain difficulties in some aspects of the measurements. The data extraction was cumbersome, even though it could be done rapidly. The monolithic brass block cell enclosure lacked flexibility for changing suspension properties as needed to accommodate alternate measurement priorities. For example, experiments differ on requirements of highest sensitivity or of higher density range. Temperature control was marginal for highest precision. Sensor noise prevented operation at the extremely low buoy amplitudes (< 5 nm) that would sometimes be desired.

This article describes our improvements in a newly designed instrument which attempts to meet these difficulties. In the next sections, we briefly review the method of operation and the main features of the basic system. Following this, we describe the new design and present a measurement of intrinsic viscosity which illustrates its performance as a viscometer.

I. BACKGROUND

To reasonable accuracy for small motion, a magnetically suspended object acts as a mass on a spring.[1] Damping, either electronic or through viscous drag, is necessary for the servoloop to be stable.[4] In the case of the oscillating buoy viscometer, essentially all the damping is supplied by the fluid in which the buoy is suspended. Consequently the phase lag of the buoy relative to some sinusoidal driving force is directly related to the viscosity of the fluid. With this assumption, we write the differential equation of vertical motion of the suspended, driven buoy as

$$m\ddot{z} + b\dot{z} + kz = F \sin \omega t. \tag{1}$$

The familiar solution for this forced, damped harmonic oscillator equation is

$$z = A \sin(\omega t + \beta), \tag{2}$$

where

$$A = F\left[m^2(\omega^2 - \omega_0^2) + b^2\omega^2\right]^{-1/2}, \tag{3}$$

and

$$\sin \beta = -b\omega\left[m^2(\omega^2 - \omega_0^2) + b^2\omega^2\right]^{-1/2}, \tag{4}$$

with $\omega_0^2 = k/m$. The ratio of Eqs. (3) and (4) yields

$$F \sin(\beta)/A = -b\omega, \tag{5}$$

which is the working equation for our instrument.

Boundary layer effects[1,5,6] slightly complicate the relationship between b and the viscosity as will be discussed, but our new computer-controlled instrument is able to account for them in real time if desired.[7]

In practice we have been interested in a relative viscosity (η/η_0) range from 1.0 to 2.0, or occasionally from 0.7 to 1.0. Here η_0 is the viscosity of pure water at 20.000 °C. The buoy is a 3-mm-diam polypropylene sphere in which a 1-mm-long by $\frac{1}{2}$-mm-diam cylindrical Sm–Co magnet is placed. The ef-

 0034-6748/87/122306-07$01.30

fective density of the buoy ranges from about 1.1 to 1.8 g/cm^3, depending on the void left along with this magnet. The magnetic vertical drive signal is generated by the same coils that provide the suspension. A precision generator (Hewlett–Packard model HP3325A), usually at 500-μV rms and 3.8 Hz, is summed into the servosuspension loop. Response has been found to be linear to below 10-nm amplitude, but the sensor noise at that level causes the phase signal to be noisy.[1]

A trigger signal synchronous with the generator drive signal is used for the reference channel of the lock-in amplifier (Ithaco model 393) which serves as a response amplitude and phase lag analyzer. The buoy position and motion are sensed as a shadow on a split photodiode detector, the output of which serves as the feedback signal to the amplifier driving the suspension coils. (In the new instrument it is a quadrant photodetector.) Figure 1 is a diagram of the system, including the computer-controlled data-acquisition components.

Water at 20 °C has a fractional temperature coefficient of viscosity of $\Delta\eta/\eta = 0.0245$ per degree C. This implies a need for temperature control of the sample to ~ 4 mK in order to maintain precision at the level of 10^{-4}. A Tronac model PTC-41 controller maintains its 55-l bath to within 1 mK of 20.000 °C as measured by a Brooklyn precision mercury thermometer with 2-mK divisions. A pumping system circulates this water through the aluminum housing into which the sample cell is set and located with Delrin mounts. The photodiode preamplifier is mounted as a monolithic unit to the housing, to further stabilize the front-end electronic gain and dc voltage level.

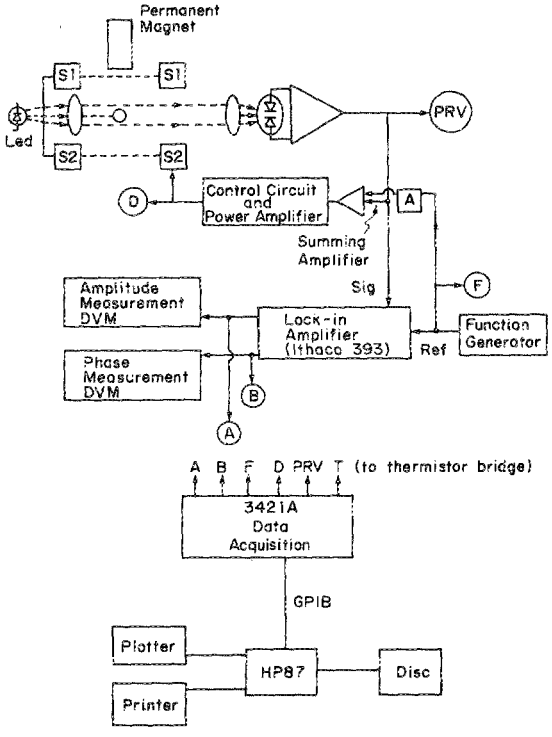

FIG. 1. Schematic diagram of oscillating buoy system. Frequency F is usually set and entered as a constant in the software. S1 and S2 are the "crossed coil" support pair. For simplicity the photodiode is shown only as a pair, but is really a quadrant detector with a "front–back" readout.

II. DETAILED DESIGN OF THE NEW INSTRUMENT

Figure 2 shows pictures which are external and internal views of the main housing of the new instrument. It is made almost entirely of aluminum, with no magnetic materials to distort the suspension field. The outer body dimensions are 17 cm square by 13 cm high. It consists of accurately machined aluminum plates with brass guide pins and brass screws. The two suspension coils are mounted to the insides of the top and the bottom and precision spacers can be inserted to change the suspension characteristics by changing the coil separation. Large water channels in the top and bottom plates allow sufficient flow of water to keep the housing temperature close to the 20 °C bath temperature.

Cylindrical Delrin inserts hold the precision rectangular cell to within 0.02 mm of a specified position. Thus, once the magnetic properties of the suspension are determined at the cell location they can be retained on disassembly and reassembly. Once absolute transfer functions are obtained

(a)

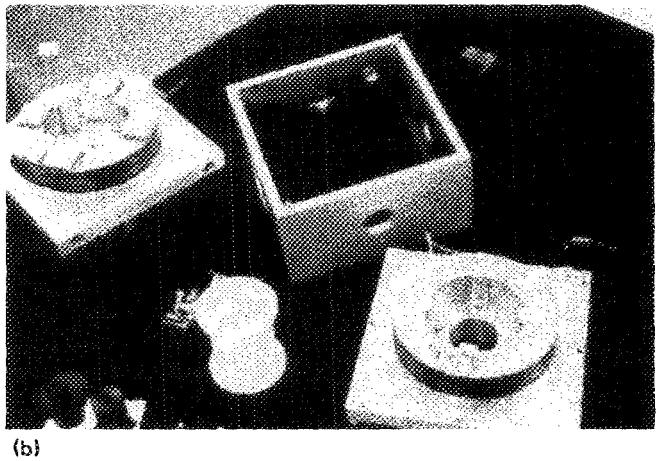

(b)

FIG. 2. Photographs of the viscometer–densimeter. (a) Overall view showing housing with several optical tubes and the temperature control water lines removed. Electronic controls show at the rear, but the data-acquisition system is out of the picture. (b) Exploded view of interior of the housing and some of the internal components. See text for more detailed description.

they can be retained and the instrument can be used as an absolute viscometer, although to somewhat lower accuracy.

The cell, unlike our previous cylindrical ones,[1] is a commercially available rectangular one with precision quartz sides. It has a 5-×5-mm square inside cross section and 7.5-mm inside height. Its vertical position can be adjusted and maintained to keep the buoy centered in whatever sample depth is used. We typically use a depth of 5 mm so the sample volume is 125 μl. Since light scattering from the cell bottom or the under surface of the top of the liquid can give undesirable effects on the signal, careful collimation of the beam is important. The flat sides of the new cells have removed much of the deleterious behavior that we reported with the old circular cross sections.

Both the infrared led suspension light source and the photodiode are in tubes with lenses in front for focusing. The tubes can be slid smoothly in and out to optimize the optical properties. We have found a slightly converging beam across the spherical buoy to give the most stable suspension.

The photodiode is a four-quadrant unit, feeding four independent low-noise operational amplifiers. Electronic summation circuitry allows both vertical and horizontal position sensing, as shown in Fig. 3. Comparing the sum signal from the two top quadrants with the sum of the two bottom quadrants gives the vertical position signal. Comparing the sum of the front quadrants with the sum of the rear two gives a horizontal signal in the front-to-back direction. (We have the support light beam going from the left to the right.) This sensing and centering in the third direction was an important missing element in the original design. The quadrant detector is often used this way. Another viscometer[2] uses it in a related but slightly different way.

Vertical location and centering of the buoy in the left–right direction are done optically. A high-quality telescope is threaded into the precise center of the front of the square housing for observing the remaining dimension of the buoy position. With an appropriate objective lens it focuses the internal cell width, 5 mm, exactly onto a 100-division scale.

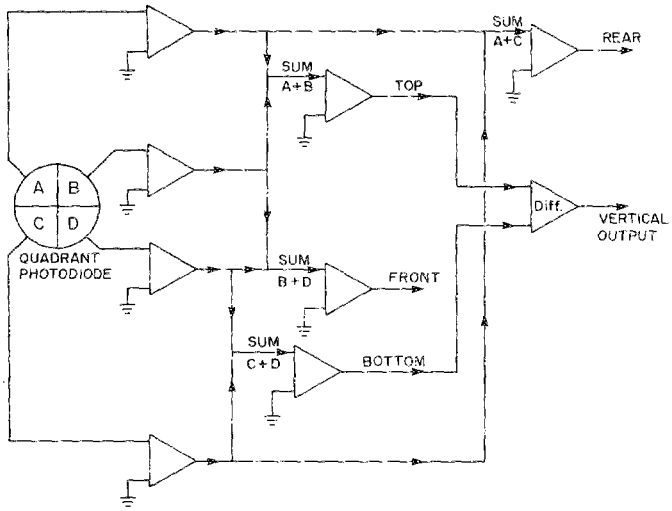

FIG. 3. Simplified schematic diagram of preamplifier circuit for quadrant detector.

With green backlighting (a color for which the silicon photodiode is very inefficient) we can easily see the 3-mm- (60-division) diam buoy. Motion to $\frac{1}{10}$ division or 5 μm is easily resolved. Electronic sensing of the vertical and transverse (to the beam) position and motion are much more sensitive, but this optical observation is sufficient and it gives a satisfying direct view. The 5-μm inaccuracy is about $\frac{1}{200}$ of the spacing between the edge of the buoy and the cell wall.

The use of an infrared led (ired) light source has provided much of an observed 80-fold increase in signal over the original visible light led. Part of this increase is due also to the improved spectral match with the photodetector, and part is due to somewhat better focal properties. Not all of this gain can be used, however, as the limited "dynamic headroom" of the ± 12-V range of the operational amplifiers required us to use lower electronic gain to avoid saturation. Nevertheless, the useful signal-to-noise improvement was about 10 times. The present ired light source is not totally satisfactory as it seems to have poorer axial beam symmetry than the visible light led. The quadrant detector and adjustable positioning tubes make such measurements of beam profile a relatively precise procedure.

III. THE MAGNETIC SYSTEM AND MOTIONAL STABILITY

The magnetic components of the new instrument have been given much attention and we will detail the related design principles here. In addition to the buoy the magnetic elements consist of the main "crossed coil" support and drive system,"doughnut" ferrite bias magnets just above the cell, and a bias coil mounted above these. The crossed coil system is a parallel pair such as a Helmholz pair but with oppositely directed currents. With appropriate spacing, these form a linear quadrupole having zero magnetic field at the center and a maximum gradient there.

Figure 4 shows the magnetic field (a) and vertical field gradient (b) on the axis of an ideal coil system of this type. Here the scaling is for a pair of coils of one turn each, with 1 A current and spaced 1 m apart. A variety of radii are shown in meters. For scaling to any given coil pair one uses the axial field equation

$$B_z = \frac{\mu_0 N I \rho^2}{2}\left(\frac{1}{(z^2+\rho^2)^{3/2}} - \frac{1}{[(2z_0 - z)^2 + \rho^2]^{3/2}}\right), \quad (6)$$

where μ_0 is the permeability of free space, N the number of turns in each coil, I the current, z the position above the plane of the bottom coil, ρ the coil radius, and $2z_0$ the coil spacing. The gradient equation is

$$\frac{\partial B_z}{\partial z} = \frac{-3\mu_0 N I \rho^2}{2} \times\left(\frac{z}{(z^2+\rho^2)^{5/2}} - \frac{(2z_0 - z)}{[(2z_0 - z)^2 + \rho^2]^{5/2}}\right). \quad (7)$$

The gradient at the center, $z = z_0$, is

$$\left.\frac{\partial B_z}{\partial z}\right)_{z_0} = \frac{-3\mu_0 N I \rho^2 z_0}{r_0^5}, \quad (8)$$

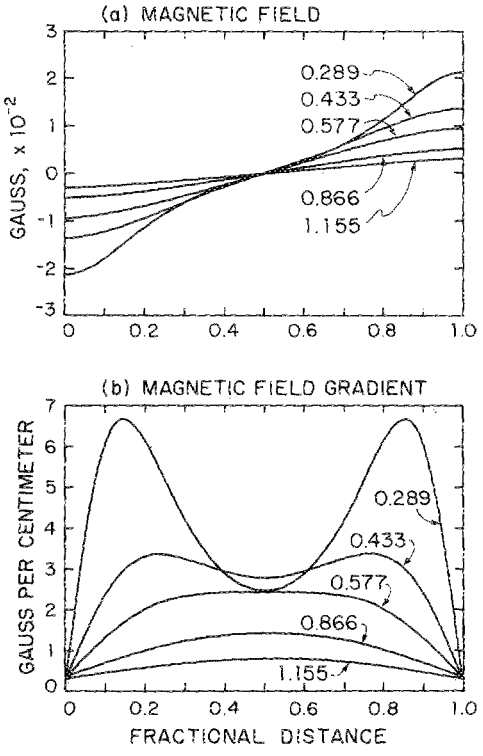

FIG. 4. Plot of vertical magnetic field (a) and gradient (b) for "crossed coil" pair to show trends. Scaled so that each coil has 1 A and the coils are spaced 1 m apart. Curves are shown for five different radii, in meters. See text for equations to scale to realistic dimensions.

where $r_0^2 = \rho^2 + z_0^2$.

For a permanent magnet buoy such as the Sm–Co one used here, the force, $F = \mathbf{M}\cdot\nabla\mathbf{B}$ is linear with current.[4] Here $\mathbf{M}$ is the buoy magnetic moment. For a fixed spacing the gradient at the center (where the buoy is located) has a maximum for $\rho/z_0 = \sqrt{2/3} = 0.8165$, i.e., a ratio of diameter to spacing of 0.8165. The "flattest" gradient[8] occurs when this ratio is $2\times 0.577 = 1.154$, at a sacrifice of about 15% of the force.

For maximum stability of the buoy drive-phase relationship both the mechanical and magnetic properties should have a high degree of (vertical) axial symmetry: (1) a departure of the buoy shape from sphericity, coupled with axial asymmetry of the optical suspension beam, gives a miniature "propeller" effect, (2) misalignment of the buoy magnetic drive axis with the gravitational axis (composed of the center of mass and center of buoyancy) will give tilting motion about a horizontal axis (we observe this at times as a high-frequency series of harmonic spikes in the power spectrum of the preamplifier output signal, i.e., the vertical position signal), and (3) the need for accuracy in centering the Sm–Co magnet within the polypropylene sphere is apparent.

The greatest sensitivity of the measurement to density change and to certain magnetic–mechanical anomalies occurs when the buoy and sample density are nearly alike. This is sometimes a desired experimental situation. It will be discussed first with respect to the density (static buoy) measurement. Then the effect of anomalies on the oscillations will be considered.

As an extreme example we can take a solution which has almost exactly the density of the buoy. Then as reactions change the density of the solution it will in some cases lead to a reversal of the gravitational force direction, i.e., a sinking buoy becomes a floating one, or vice versa. Since the magnetic field changes direction at the center of the crossed coils that is an unstable point of orientation of the magnetic moment of the buoy. Taken together with the unstable density situation just described, this implies a tendency for the buoy to flip over. Therefore, a "bias coil" or bias permanent magnet, or both are needed to move the magnetic reversal point away from the buoy position. This overcomes the unstable tendencies and keeps the alignment of the axis of the buoy in a given direction. A bias field is generally a better solution to this than forcing the buoy to have an equilibrium point above or below the center of the coil system.

A further complication arises when the Sm–Co magnet is not located in the center of the sphere. The failure to be centered transversely causes the magnetic drive force to be off line of the center of the viscous drag force and a twisting motion will occur. The failure to be centered longitudinally is a slightly more complicated problem. In such a case, an oscillating magnetic force centered at the center of the magnet will not be centered in the sphere, although the oscillating viscous drag force will be. For the small motions we have used, this has not led to observable effects at the level of 10^{-3} in precision, but at some level these small, driven rotations would be expected to be a problem.

We use both permanent magnets and a coil for the biasing field, and we are still experimenting with it. The permanent magnets are ferrite "doughnuts" of 7-mm o.d., 3-mm i.d., and 7-mm height, magnetized along the axis. The field just at the top is about 300 G. The cell fill tube goes through the center hole. Usually one such magnet is located 3.5 cm above the center of the buoy, although with denser solutions two magnets at 4.5–5 cm distance give better stability. These magnets have precision dimensions and are located in a precision Delrin tube for centering, with precision Delrin spacers for vertical location. Mechanical stability of this system is crucial for high-precision viscosity and density measurements.

A solenoid, 8 cm long by 5.5 cm mean diameter, provides the added, adjustable biasing field. This is convenient for calibration, but the 200 mA through its 300 turns constitutes an appreciable heat load to the precision temperature control system. The bottom of this solenoid is located just above the ferrite magnet and concentric with it. Since the coil lacks perfect axial symmetry, a transverse adjustment mechanism with micrometerlike screws allows fine centering corrections to be made on the buoy position.

The biasing field, although necessary for stability, adds one undesirable aspect with its gradient. This gradient causes a "neutral density buoy" (one with the same density as the solution) to demand current in the main servoloop in order to stay in the centered vertical position. This equilibrium current is another heat load which must be handled with the temperature control system, with its limited heat removal capabilities. In experiments where a relatively small density change is to occur, an optimum choice of buoy

weight (i.e., effective density) can be made so that the gravitational plus buoyancy force just matches the magnetic biasing field alone, so that the main coil pair can operate near zero power.

It is clear that in the general situation an adjustable biasing field, whatever its heat load problems, adds considerable flexibility in the experimental strategy.

IV. LIMITS OF BOUNDARY LAYER CORRECTIONS

In our original work, the calibration and other data were painstakingly read and analyzed by hand, and the analyses were as a result somewhat limited. Since the adoption of computer readout and control,[7] we have been able to take and analyze huge amounts of calibration and other data as well as some of the internal equipment parameters. One of the immediate benefits was the ability to see slight curvature in the calibration lines in some conditions and to be able to correct for it exactly by inclusion of boundary layer effects in the calibration program. Here we will present a simple measurement series which permits us to determine the limits of application of the first-order corrections.

The question of boundary layer effects on the buoy motion has been discussed in general[5] and specifically with respect to a sphere executing a variety of motions in a fluid, particularly translational oscillations.[6] In Ref. 1 this was brought out in the present context. Essentially the boundary layer problem is treated by assuming the sphere has a complex velocity. The result is that there is an increased effective mass for a sphere of radius r, which is approximately given by

$$m^* = m[1 + (1/2)(\rho/\rho')(1 + 9/2\delta/r)], \qquad (9)$$

where ρ is the fluid density, ρ' the buoy density, $\delta = \sqrt{2\nu/\omega}$ a boundary layer parameter, and ν is the kinematic viscosity. The result also contains an increased drag coefficient, given approximately by

$$b^* = 6\pi\eta r(1 + r/\delta). \qquad (10)$$

In our operating regime, where $0.13 < \delta/r < 0.4$ we would expect the boundary flow to be more dissipative, i.e., to modify b more than m. That is observed to be the case.

The approximations leading to Eqs. (9) and (10) are met only when the nonlinear term of the Navier–Stokes equation $(\mathbf{v}\cdot\nabla)\mathbf{v}$ can be neglected. The conditions for this are[1,6] that: $r > \delta$, $r^2\omega \gg \nu$, and $r \gg A$. In the test reported here, the drive amplitude was varied for a sample of pure water. We used four different drive levels, regimes labeled A to D in Fig. 5. Table I lists the parameters and results derived from this data. Measured values of $H = \eta/\eta_0$ in the table are averaged values calculated for equilibrium regions by the computer rather than the less accurate values that could be obtained from the plot. In each case, the estimated drive amplitude is taken from the lock-in amplifier output voltage amplitude and a previously calibrated height-to-voltage transfer function. The preamplifier output spectrum was taken simultaneously with a spectrum analyzer, and it was evident that at the highest drive level the harmonic content was such as to make this particular amplitude estimate unreliable. For region C, visual observation through the calibrated telescope gave a reasonably good confirmation of the calculated amplitude.

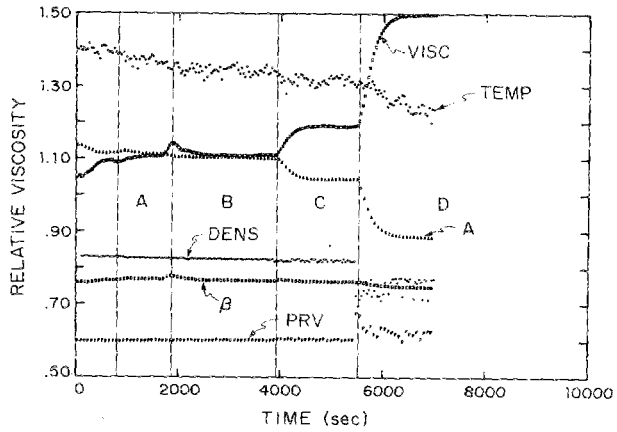

FIG. 5. Computer real-time plot of viscosity, temperature, buoy amplitude, density, phase lag, and preamplifier suspension signals. Time regimes A–D are for succeeding increases in drive amplitude, as discussed in text. On each change the lock-in amplifier range for amplitude A was changed. See text for discussion of temperature scale.

One can conclude from Table I that at some buoy motional amplitude between 10 and 90 μm the nonlinear effects of drive amplitude have become appreciable. The amplitude independence required for Eqs. (9) and (10) above no longer holds and the first-order boundary corrections are not adequate. In all runs we now maintain the drive amplitude well below 10 μm.

V. TEMPERATURE CONTROL

The cooling water flow through the housing must remove most of the heat generated by the suspension and bias coils. The former varies with the sample density and the latter is constant. For perfect heat transfer, the power that could be removed for a given temperature rise ΔT would be given by

$$P = cQ\Delta T \quad \text{W}, \qquad (11)$$

where $c = 4.2$ J/g °C and Q is the mass flow rate, which for water is essentially the volume flow rate. In our instrument this is about 6 cm^3/s. This corresponds to about 40 mK per watt dissipation in the instrument.

The mass of the aluminum housing, with appendages, is about 7 kg. The heat capacity equation

$$\Delta Pt = cm\Delta T \quad \text{J}, \qquad (12)$$

can be used to estimate the rate of temperature change for a step shift ΔP in power dissipation. Using $c = 0.907$ J/g °C for aluminum, the housing temperature change rate in mK/s would be $\Delta P/6.35$.

A precision thermistor is mounted with good thermal contact to the interior of the aluminum housing, near the sample cell. It is connected to our adaptation of a four-scale bridge circuit.[9] This was calibrated against a Brooklyn Thermo Co. model 8N292 mercury thermometer. On the most-used bridge scale the calibration is -8.5 mK/mV. With this calibration the observed temperature drift rate of Fig. 5, which was about 15 mV over 7000 s, is roughly 0.02

TABLE I. Viscometer behavior as a function of drive level. $f_0 = 4.32$ Hz, $f = 4.75$ Hz, filter time constant = 125 s.

Drive region	Voltage drive into loop (V rms)	Estimated buoy amplitude (μm)	Lock-in voltage amplitude (A)	Phase lag (°)	Measured $H = \eta/\eta_0$	Visually estimated amplitude (μm)	Second-harmonic amplitude[a] (%)
A	0.001	0.98	6.13[b]	27.0	1.107	—	<0.01
B	0.01	9.7	6.040[b]	26.5	1.108	—	<0.1
C	0.9	87	5.45[b]	26.3	1.189	60	2
D	1.0	[c]	[c]	[c]	[c]	800	14

[a] As measured at preamplifier output with HP3582A spectrum analyzer.
[b] Gain switched by factors of 10, as required.
[c] Unreliable.

mK/s. This rate represents a total power shift of about 120 mW. The total temperature rise, about 130 mK, would change the relative viscosity about 0.003. This is insignificant in this particular run but it would be disastrous in a sensitive viscosity or density measurement. With insulation and equilibration, we commonly observe temperature changes of the viscometer housing less than 5 mK over complete runs. Even this amount could be excessive in some cases, and we have computer programs now[7] which automatically make a first-order correction for the observed temperature.

VI. A MEASUREMENT OF INTRINSIC VISCOSITY

Intrinsic viscosity $[\eta]$ is a characteristic of proteins and other molecules related directly to their ability to disturb flow and indirectly to their size and shape.[10] In this section, we will present a measurement of $[\eta]$ for 2-propanol, as an illustration of the way in which our computer-analyzed data system can deal with some troublesome aspects of the technique.

Einstein[11] showed that the viscosity η of a dilute solution of rigid spherical particles is related to the viscosity η_1 of the solvent by

$$\eta = \eta_1(1 + 2.5\phi), \tag{13}$$

where ϕ is the fractional volume occupied by the spheres. Hence, the second term is proportional to the concentration of the spheres. Rotation of nonspherical molecules causes a disruption of the laminar flow (and, therefore, of the viscosity) more than their actual volume, so that the second term can be replaced with a power series in concentration C. It is common to make two definitions in dealing with this further. The "specific viscosity" η_s is defined as the excess of the relative viscosity over unity, $\eta_s = H - 1$. The "intrinsic viscosity" $[\eta]$ is defined as η_s/C, for reasons that will become apparent. A rearrangement of Eq. (13) gives

$$\eta_s = H - 1 = 2.5\phi = kC + k'C^2 + \ldots . \tag{14}$$

Dividing by C this is

$$[\eta] = k + k'C + \ldots . \tag{15}$$

The information about the molecular asphericity is contained in k, which is, in fact, the theoretical value of $[\eta]$. Simha has shown[12] that both prolate and oblate spheroids increase viscosity in proportion to their eccentricity. Therefore, the value of k is a direct measure of the eccentricity. The value of k' is interpreted as a measure of the change of eccentricity with concentration.

As many as five methods have been used for obtaining the intrinsic viscosity by extrapolation to zero concentration,[10] most of them being forms of these equations manipulated to minimize the errors introduced by two constraints. Equation (14) illustrates the constraints that are at issue in the extrapolation method. At high concentration, the nonlinear terms are important and present an unknown aspect of the molecular conformation into the problem. At low concentration, H closely approaches unity so that there is large fractional error in the value of η_s and, therefore, also in $[\eta]$. The fitting of a straight line to the data, whose slope is the desired value k, must appropriately account for these two constraints.

Viewing Eq. (15) as an experimental one, we can estimate the expected experimental fractional error in $[\eta]$ due to errors in η and in C. This yields

$$\frac{d[\eta]}{[\eta]} = \frac{d\eta_s}{\eta_s} + \frac{dC}{C} = \frac{d(H-1)}{H-1} + \frac{dC}{C}, \tag{16}$$

where the sign of the second term has been reversed to deal with the magnitude of the fractional error in C, the usual statistical assumption of independence of the two errors. If the viscometer can measure H to accuracy of 0.001 and C to that level, then the first term in Eq. (16) has a 100% error expectation at a concentration for which $H = 1.001$.

We have used 2-propanol in water as our experimental solution for illustration. A quadratic fit of the value of $H - 1$ to the tabulated data in the concentration region below 5%[13] yields

$$H - 1 = 0.0524C + 0.000084C^2, \tag{17}$$

where C is given in percent by weight. For very low values of C the linear term will suffice. We see that the slope is roughly 1 in 20. A viscometer precise to 0.1% will contribute an error to the first term of Eq. (16) of 100% at $C = 0.02\%$, 10% at $C = 0.2\%$, and 1% at $C = 2\%$. If C itself is measured to 0.1% its error can be ignored in this extrapolation.

Table II lists the results of one such procedure with our instrument. In this run, we started with an approximately 8% solution. Each subsequent datum followed a 50% dilution with pure water. The errors in C are rather significant in this run. (The sample was 125 μl and we used a 500-μl syringe so that the dilution accuracy was probably no better than 5%. For calibrations of the instrument we use careful

TABLE II. Measurement of intrinsic viscosity of 2-propanol.

	C (%)	H	$H-1$	k	$(k-\langle k\rangle)/\langle k\rangle$
1	8.228	1.4987	0.4987	6.061	0.078
2	4.114	1.2208	0.2208	5.367	−0.045
3	2.057	1.1238	0.1238	6.018	0.071
4	1.028	1.0538	0.0538	5.233	−0.069
5	0.514	1.0272	0.0272	5.292	−0.059
6	0.257	1.0157	0.0157	6.109	0.087
7	0.129	1.00344	0.00344	2.667	−0.526
8	0.064	1.00337	0.00337	5.266	−0.063

Mean (8 pts)	$[\eta]=\langle k\rangle=5.252$	
Std dev		1.113
Std dev of the mean		$1.113/\sqrt{8}=0.394$ (7.5%)
Mean (pts 1–6)	$[\eta]=\langle k\rangle=5.680$	
Std dev (1–6)		0.422
Std dev of the mean (1–6)		0.172 (3.0%)

weighing techniques so that the calibration accuracy is not limited in this way.) From the table, discarding points for which $C<0.2$, we find the mean value 5.680 for the intrinsic viscosity of 2-propanol. The rms deviation of the points is 0.422 (7.4%) and the standard deviation of the mean is 0.172 (3.0%). Our value can be compared with one derived from the tabulated viscosity data on 2-propanol solutions. From Eq. (17) it can be seen that the rough procedure of fitting to the tabulated data (which was given only at 1% intervals) yields a value of 5.24 for k and 8.4 for k'. This value for k' is highly questionable.

If it is assumed that the data are of sufficient quality that the second-order term in C might have significance, the data can be fit as a straight line through a plot of intrinsic viscosity vs C. A slope of zero would imply that k' is insignificant. With our data this procedure yields an intercept of 5.491 and a slope of 0.0558 when the concentration is in fraction by weight. The rms deviation of the points is lowered to 0.354 (6.4%) but this nonzero slope of the fit line is in fact not significant.

ACKNOWLEDGMENTS

We wish to acknowledge support from a National Institutes of Health Grant No. NIH 5 R01 GN32201. We also wish to thank Professor Donald W. Kupke of the Biochemistry Department of the University of Virginia for many discussions and suggestions.

[1] C. H. Leyh, M. Sc. thesis, University of Virginia, 1981; C. Leyh and R. C. Ritter, Rev. Sci. Instrum. **55**, 570–577 (1984).
[2] B. Gauthier-Manuel, J. Phys. E **17**, 1183–1186 (1984); *ibid.*, pp. 1177–1182.
[3] Z. Guozhen and X. Laoli, Rev. Sci. Instrum. **56**, 1639–1642 (1985).
[4] W. S. Cheung, C. H. Leyh, and R. C. Ritter, in *Proceedings of International Symposium on Precision Measurement and Gravity Experiment*, Taipei, Taiwan, edited by W.-T. Ni (National Tsing Hua University, Hsinchu, Taiwan, 1983), pp. 81–102.
[5] H. Schlichting, *Boundary-Layer Theory*, 7th ed. (McGraw-Hill, New York, 1979), p. 428.
[6] L. D. Landau and E. M. Lifshitz, *Fluid Mechanics* (Pergamon, New York, 1959), p. 88.
[7] R. C. Ritter and D. Sullivan, Computer-Controlled Viscometer–Densimeter (to be submitted).
[8] H. Zijlstra, *Experimental Methods in Magnetism, I* (North-Holland, Amsterdam, 1967), pp. 34–38.
[9] P. H. Sydenham and G. C. Collins, J. Phys. E **8**, 311–315 (1975).
[10] D. E. McMillan, Biopolymers **13**, 1367–1376 (1974).
[11] A. Einstein, in *Investigations on the Theory of Brownian Movement*, edited by R. Furth (Methuen, London, 1926), p. 54.
[12] R. Simha, J. Phys. Chem. **44**, 25–34 (1940).
[13] *C. R. C. Handbook of Chemistry and Physics*, 66th ed., edited by R. C. Weast (CRC Press, Boca Raton, Florida, 1985), p. D-249.